



Article

A Hybrid Machine Learning Model Coupling Double Exponential Smoothing and ELM to Predict Multi-Factor Landslide Displacement

Xing Zhu ¹, Fuling Zhang ^{1,2,*} , Maolin Deng ², Junfeng Liu ^{1,3}, Zhaoqing He ¹, Wengang Zhang ⁴ and Xin Gu ⁴

- ¹ State Key Laboratory of Geohazard Prevention and Geoenvironment Protection, Chengdu University of Technology, Chengdu 610059, China; zhuxing15@cdut.edu.cn (X.Z.); liujunfeng@stu.cdut.edu.cn (J.L.); hezhaoqing@stu.cdut.edu.cn (Z.H.)
- ² Hubei Province Disaster Prevention and Mitigation Engineering Technology Research Center, China Three Gorges University, Yichang 443002, China; dmltop@163.com
- ³ College of Computer Science and Cyber Security (Oxford Brookes College), Chengdu University of Technology, Chengdu 610059, China
- ⁴ School of Civil Engineering, Chongqing University, Chongqing 400044, China; zhangwg@ntu.edu.sg (W.Z.); guxin@cqu.edu.cn (X.G.)
- * Correspondence: fulingzhang@stu.cdut.edu.cn; Tel.: +86-028-84073193

Abstract: The deformation of landslides is a non-linear dynamic and complex process due to the impacts of both inherent and external factors. Understanding the basis of landslide deformation is essential to prevent damage to properties and losses of life. To forecast the landslides displacement, a hybrid machine learning model is proposed, in which the Variational Modal Decomposition (VMD) is implemented to decompose the measured total surface displacement into the trend and periodic components. The Double Exponential Smoothing algorithm (DES) and Extreme Learning Machine (ELM) were adopted to predict the trend and the periodic displacement, respectively. Particle Swarm Optimization (PSO) algorithm was selected to obtain the optimal ELM model. The proposed method and implementation procedures were illustrated by a step-like landslide in the Three Gorges Reservoir area. For comparison, Least Square Support Vector Machine (LSSVM) and Convolutional Neural Network–Gated Recurrent Unit (CNN–GRU) were also conducted with the same dataset to forecast the periodic component. The application results show that DES-PSO-ELM outperformed the other two methods in landslide displacement prediction, with RMSE, MAE, MAPE, and R^2 values of 1.295mm, 0.998 mm, 0.008%, and 0.999, respectively.

Keywords: landslide displacement prediction; Extreme Learning Machine; Variational Modal Decomposition; machine learning



Citation: Zhu, X.; Zhang, F.; Deng, M.; Liu, J.; He, Z.; Zhang, W.; Gu, X. A Hybrid Machine Learning Model Coupling Double Exponential Smoothing and ELM to Predict Multi-Factor Landslide Displacement. *Remote Sens.* **2022**, *14*, 3384. <https://doi.org/10.3390/rs14143384>

Academic Editors: Jean-Philippe Montillet, Rui Fernandes, Xiaoxing He, Zhao Li, Feng Zhou and Gaël Kermerrec

Received: 9 June 2022

Accepted: 11 July 2022

Published: 14 July 2022

Publisher's Note: MDPI stays neutral with regard to jurisdictional claims in published maps and institutional affiliations.



Copyright: © 2022 by the authors. Licensee MDPI, Basel, Switzerland. This article is an open access article distributed under the terms and conditions of the Creative Commons Attribution (CC BY) license (<https://creativecommons.org/licenses/by/4.0/>).

1. Introduction

Landslide is one of the most common, frequent, and detrimental geo-hazards around the world. It has caused great harm to human lives, properties, and infrastructures. The Three Gorges Reservoir (TGR) area of China, a 660 km-long area along the Yangtze River behind the large Three Gorges Dam, is exposed to geo-hazards due to the volatility of hydrological conditions like seasonal precipitation and periodical reservoir water level (RWL) [1–3]. Landslide is the most representative term among those geo-hazards, with over 4200 potential landslides distributed in the TGR area [4]. The fatal Qianjiangping landslide, with 14 million m³ materials, was reactivated as the RWL rose to 135 m after the initial impoundment of the TGR in 2003. In this catastrophic landslide, a 30 m high impulse water wave was triggered, 24 people died, and 129 buildings and many crafts were destroyed [5]. To avoid or reduce damage induced by landslides, an early warning system has been gradually established and improved in this area to effectively and timely identify the large deformation of the potential landslides, and collect the reservoir water

level and rainfall data [4]. However, a landslide is a complex and non-linear system, and the mechanisms might be not yet clearly understood and different from each other. As the direct output of this system, displacement of landslides is the result of the compound action of the inherent geological circumstances and mechanical complexity of landslides, as well as external triggering factors over time. As a critical component of the landslides early warning system, displacement prediction of landslides in advance has been proved an effective way for early prevention of landslide geo-hazards and avoiding the loss of property and lives [6,7]. However, accurate prediction of landslide displacement triggered by multi-factors is still challenging.

As a result of the prosperity of artificial intelligence, researchers have devised a lot of different intelligent data-driven machine learning (ML) algorithms to solve nonlinear complicated problems in many fields. Several representative ML models were also conducted to forecast landslide displacement. Artificial neural network (ANN) [8], random forest [9], support vector machine (SVM) [10–12], extreme learning machine (ELM) [13–16], and the long short-term memory (LSTM) neural networks [17–20] have been broadly studied and successfully utilized in landslide displacement prediction. According to their real applications, those popular models can be classified into two categories: univariate forecasting model and multivariate forecasting model. The univariate forecasting model simply takes the preceding displacement as the indicator for predicting the future displacement of landslides, while the multivariate forecasting model can consider external triggering factors of landslide deformation as well. Landslide total surface displacement can be split into trend and periodic parts [21]. The trend component can be forecasted by the univariate forecasting model and the periodic component which is affected by external influences can be forecast with the multivariate forecasting model. Therefore, the multivariate model may accomplish a smaller forecast error than the univariate model since the influencing factors are taken carefully into account [6,22].

In this study, we proposed a hybrid machine learning model coupling the double exponential smoothing (DES) and the particle swarm optimization-extreme learning machine (PSO-ELM), a novel artificial neural network architecture, to forecast the landslides displacement which is frequently strongly affected by reservoir water level changes and rainfall. The Baijiabao landslide in the TGR area, which has a step-like (intermittent) deformation characteristic, was regarded as a case study herein. On the grounds of time series decomposing and fully understanding the deformation mechanism of this landslide, six major influences related to RWL and rainfall were input into the prediction model. The least-square support vector machine (LSSVM) and convolutional neural networks-gated recurrent unit (CNN-GRU) is also applied for comparison with the ELM model. The prediction results demonstrate that the ELM model has a higher predictive performance than the other two models.

2. Methodology

2.1. Procedure of the Proposed Model for Landslide Displacement Prediction

Figure 1 shows a schematic plot of the proposed hybrid machine learning model for landslide displacement prediction. The wireless sensors deployed on the landslide in TGRA generally include reservoir water level gauge, rainfall gauge, and global navigation satellite system (GNSS). The former two devices are employed to automatically monitor the external triggering factors, such as RWL and rainfall, which have a strong contribution to the step-like deformation characteristic of landslides [23]. The GNSS is implemented to monitor the ground displacement of landslides. First, the total surface displacement of the landslide observed by GNSS was divided into trend components and periodic components by variational mode decomposition. The long-term trend displacement of landslides can be predicted by the univariate double exponential smoothing model, while the periodic variation component can be predicted using the multivariate extreme learning machine model with considering the external triggering factors, such as rainfall and RWL. Furthermore, to achieve the best predictive performance, the best ELM model is obtained by a particle

swarm optimization algorithm. Meanwhile, the least square support vector machine is also implemented with the same training and testing dataset for comparison with PSO-ELM. Lastly, the general criteria: the root mean squared error (RMSE), mean absolute error (MAE), mean absolute percentage error (MAPE), and determination coefficient (R^2) of prediction results were employed to evaluate the accuracy of the proposed model.

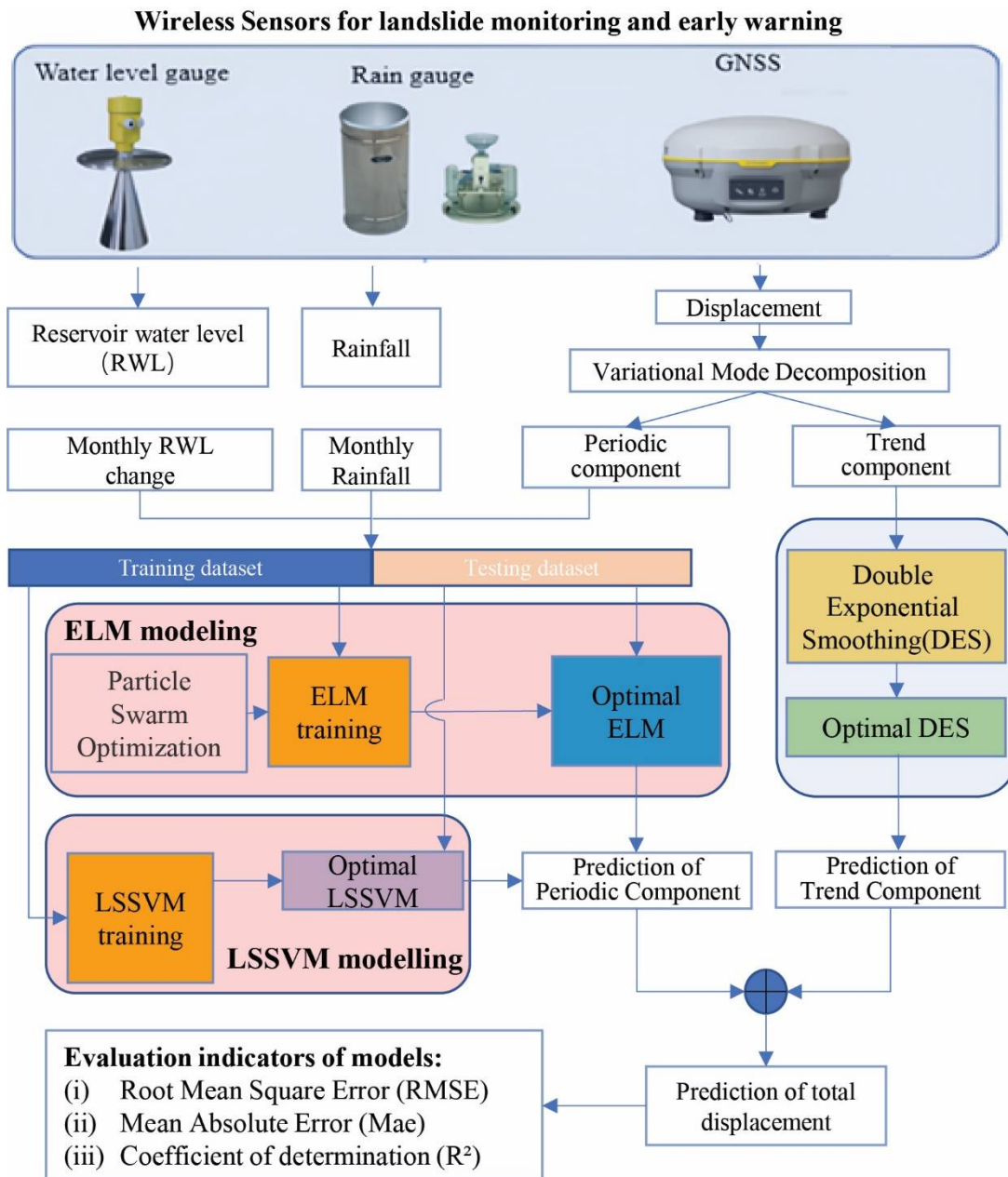


Figure 1. Procedures of landslide displacement prediction based on machine learning.

2.2. Displacement Decomposition

Due to the complex coupling action of primary influences, such as geological circumstances, and external initiating factors (e.g., precipitation, reservoir water level, snowmelt, etc.) of the slope, the movement patterns of landslides generally demonstrate non-linear evolution characteristics [21–23]. So far, many time series decomposition methods, such as double exponential smoothing [22], moving average [14], empirical mode decomposition [24], wavelet decomposition [25], Hodrick–Prescott (HP) filters [16], and variational mode decomposition (VMD) [26] have been employed to split the landslide displacement into the long-term trend component, which is influenced by the internal factors, and the

chaotic periodic variation component, which is affected by the influence triggers. It is common to adopt variational modal decomposition for modal variational problem solving and signal processing due to the adaptivity and completely non-recursive property. Compared with empirical modal decomposition (EMD) and ensemble empirical modal decomposition (EEMD), the biggest advantage of VMD is that it can determine the number of modal decompositions by itself. It has a theoretical basis and can be used to deal with nonlinear sequences with poor regularity and high complexity, decomposing the nonlinear sequences into relatively smooth subseries.

Accordingly, the cumulative displacement of landslides in TGRA can be divided into three parts as follows:

$$y_i = P_i + T_i + \varepsilon_i \quad (1)$$

where y_i is the total displacement of landslides, P_i denotes the periodic part of displacement, T_i denotes the trend part of displacement, and ε_i indicates the random noise that might be induced by observations. Due to the continuous monitoring of the surface displacement using GNSS, there are unavoidable errors and measurement noises, especially the shaking noises, in the observation data which cover up the available signals that are needed [27]. In this study, the observation noise is removed by the wavelet de-noising approach, a commonly used method, first [28].

2.3. Univariate Model: Double Exponential Smoothing (DES)

Double exponential smoothing is one of the time series analysis approaches for predicting the future trend. The basic idea of this algorithm is to introduce a weighted combination of the previous values and the last values for updating the trend of the time series through exponential smoothing. It is a suitable algorithm for predicting the trend of time series without periodic fluctuations [29]. The decomposed trend component of landslide deformation is considered, which is driven by the geological conditions rather than external triggering factors. Therefore, the DES, as a univariate prediction model, is favorable to forecast the trend displacement value of landslides based on the past observed time series. For a given time series τ_i , the key equations associated with the DES algorithm are represented as follows:

$$S_i = \alpha\tau_i + (1 - \alpha)(S_{i-1} + b_{i-1}) \quad (0 \leq \alpha \leq 1) \quad (2)$$

$$b_i = \gamma(S_i - S_{i-1}) + (1 - \gamma)b_{i-1} \quad (0 \leq \gamma \leq 1) \quad (3)$$

$$T_{i+1} = S_i + b_i \quad (4)$$

where S_i denotes the smoothed value calculated by the current observation τ_i at the time i . b_i is the best-estimated gradient at the time i . T_{i+1} is the predicted value at time $i + 1$. The initial values for S_i and b_i in DES are generally given as follows:

$$b_0 = \tau_1 - \tau_0 \quad (5)$$

$$S_0 = \tau_0 \quad (6)$$

2.4. Particle Swarm Optimization

Particle swarm optimization (PSO) is an optimization algorithm. It is a global search method proposed by Eberhart and Kennedy, an optimization algorithm that simulates the natural behaviors of organisms as well as group intelligence [30].

PSO restricts each particle to update two vectors, the velocity variable $V_i = [v_i^1, v_i^2, \dots, v_i^M]$ and the position vector $Y_i = [y_i^1, y_i^2, \dots, y_i^M]$, in the process of finding the best possible solution, where i represents the number of the particle and M is the dimension of the solution problem. The velocity vector denotes the characterized speed and direction of the motion, while the position vector determines the location of the solution in the solution room which is the basis of quality evaluation. The algorithm also requires each particle to update a vector of its historical optimal positions p_i and the population to maintain

a global optimal vector p_g . The particles update their velocity and position, calculated as follows.

$$v_{im}^{k+1} = \omega v_{im}^k + c_1 r_1 (p_{im}^k - y_{im}^k) + c_2 r_2 (p_{gm}^k - y_{im}^k) \quad (7)$$

$$y_{im}^{k+1} = y_{im}^k + v_{im}^{k+1} \quad (8)$$

where k is the count of hidden layer nodes, ω is a non-negative, inertial weight that adjusts the search range for the solution space. $P_i = [p_{i1}, p_{i2}, \dots, p_{iM}]^T$ denotes the local optimum location of the i th particle and $P_g = [p_{g1}, p_{g2}, \dots, p_{gM}]^T$ is the global best location of the swarm. c_1 and c_2 are the acceleration constant that regulates the maximum learning step. The terms r_1 and r_2 are two random functions that take values in the range $U(0, 1)$ to increase the search randomness. $[v_{min}, v_{max}]$ is the range of the velocity.

2.5. Multivariate Model: Extreme Learning Machine (ELM)

Extreme Learning Machine, firstly proposed in 2006 [31], has shown great ability in the field of prediction and comprehensive evaluation. ELM is a novel fast feedforward learning algorithm. It can randomly generate the input weights and biases to obtain the corresponding output weights of a single hidden layer neural network. The most notable characteristic of ELM is that it is faster than traditional learning algorithms while ensuring the accuracy of forecasting, especially for single hidden layer feedforward neural networks (SLFN). In recent years, ELM has shown great potential for development and application, attracting a lot of attention from researchers in academia and industry, and has achieved fruitful research results.

In the ELM model, given N arbitrarily different training samples $\{(x_i, t_i)\}_{i=1}^N$, where $x_i = [x_{i1}, x_{i2}, \dots, x_{im}]^T \in R^n$, is the input vector and $t_i = [t_{i1}, t_{i2}, \dots, t_{im}]^T \in R^m$ is the corresponding desired output vector. In a standard ELM model with n input vectors, L hidden layer neurons, and m output neurons with an activation function of $g(x)$, the mathematical model is constructed as follows:

$$T = H\beta \quad (9)$$

Which:

$$H = \begin{bmatrix} h(x_1)^T, \dots, h(x_N)^T \end{bmatrix}^T = \begin{bmatrix} g(w_1 \cdot x_1 + b_1) & \cdots & g(w_L \cdot x_1 + b_L) \\ \vdots & \ddots & \vdots \\ g(w_1 \cdot x_N + b_1) & \cdots & g(w_L \cdot x_N + b_L) \end{bmatrix}_{N \times L} \quad (10)$$

In ELM, H is also named the random feature mapping matrix, $w_i = [w_{i1}, w_{i2}, \dots, w_{in}]^T$ denotes the input weights which connect the hidden layer neuron i and the input layer neuron, b_i denotes the bias of the hidden layer neuron i , $\beta = [\beta_1, \beta_2, \dots, \beta_L]^T$ denotes the matrix of weights between the output and hidden layers, $T = [t_1, t_2, \dots, t_N]^T$ denotes the training sample expectation output matrix. After the parameters (w_i, b_i) of the hidden layer neurons are randomly initialized according to the probability of any continuous sampling distribution and given the training datasets, the hidden layer output matrix H is known and invariant, and in this way, Equation (9) is transformed into solving a minimum-parametric least-squares solution for the linear system T :

$$\hat{\beta} = H^+ T \quad (11)$$

2.6. Model Evaluation

To verify the prediction performance of the hybrid model, the root means squared error (RMSE), mean absolute error (MAE), mean absolute percentage error (MAPE), the correlation coefficient (R^2) of prediction and observation were calculated as follows:

$$RMSE = \sqrt{\frac{1}{n} \sum_{i=1}^n (y_i^* - y_i)^2} \quad (12)$$

$$MAE = \frac{1}{n} \sum_{i=1}^n |y_i - y_i^*| \quad (13)$$

$$MAPE = \frac{100\%}{n} \sum_{i=1}^n \left| \frac{y_i - y_i^*}{y_i} \right| \quad (14)$$

$$R^2 = \frac{\sum_{i=1}^n (y_i - \bar{y})(y_i^* - \bar{y}^*)}{\sqrt{\sum_{i=1}^n (y_i - \bar{y})^2 (y_i^* - \bar{y}^*)^2}} \quad (15)$$

where y_i indicates the actual observed displacement value of landslide, while y_i^* indicates the predicted displacement value of landslide, and n is the number of the data points.

3. Case Study

3.1. Baijiabao Landslide

The Baijiabao landslide is situated in the Xiangjiadian village of Zigui County. It is on the right bank of the Xiangxi River, one of the tributaries of the Yangtze River. The landslide is approximately 2.5 km away from the confluence of the Xiangxi river and 30 km away from the Three Gorges Dam [32]. The climate of this area is subtropical continental monsoon climate. The average annual precipitation and temperature range from 987 to 1326 mm and 16 and 18 °C, respectively. The rainfall season runs between April and October. Figure 2 shows the location and overall view of the Baijiabao landslide. The landslide is wide at the feet, narrow at the head, and approximately bell-shaped in the plane. The elevation and width of the upper boundary of this landslide are 280 m and 300 m, respectively. The overall slope of this landslide is approximately 16°. The length of the Baijiabao landslide from west to east is roughly 550 m. The toe of this landslide is at 125 to 135 m altitudes, which was immersed into the Xiangxi River in 2003. The thickness of the upper part is about 10 to 30 m, while the lower part is 20 to 40 m. The bedrock ridge and gully define the north and south boundary of the landslide, respectively. The volume of the sliding mass materials was estimated to be about $990 \times 10^4 \text{ m}^3$, covering an area of about $22 \times 10^4 \text{ m}^2$ [33].

Several detailed field investigations and explorations were conducted to identify the landslide features. Deposits and colluvium composed the material of the landslide. It is recognized as gravel soil [34]. The strata of the underlying bedrock belong to the Xiangxi Formation (J_1x) of Lower Jurassic and dip about 30° toward the southwest. The Xiangxi formation is dominated by alternating sandstone and silty mudstone. This formation is quite visible in the vicinity of the landslide. A crossed-section taken along I-I' line (Figure 3) is exhibited in Figure 4. The slope of the upper part of the landslide above the water is 15 to 20° while the lower part above the water has a slope angle of 5 to 10°. The lateral boundaries are defined by two gullies. The toe of the rapture surface was submerged into the reservoir in 2003.

The Baijiabao landslide experienced a significant movement, and several emergency surface monitoring monuments based on several total stations and an inclinometer ZK-1 were firstly set up to monitor the displacement of this landslide. Then, as part of the Third stage of the Professional monitoring project in TGR of the Ministry of Natural Resources, a monitoring system, as depicted in Figure 2, was implemented in October 2006 for early warning. Four GNSS displacement monitoring points, numbered from ZG323 to ZG326, were deployed to measure the surficial deformation successively. Further, another three

new GNSS monitoring devices, numbered from ZG400 to ZG402, and four crack gauges identified as C1, C2, C3, and C4 were implemented to intensify the system in 2016 and 2017, respectively. The accuracy of the GNSS device and crack meter is ± 5 mm and ± 0.1 mm, respectively. Meanwhile, a tipping bucket rain gauge was implemented to collect rainfall data automatically with a resolution of 0.2 mm per tip, the transmission time interval ranges from 5 min to 24 h.

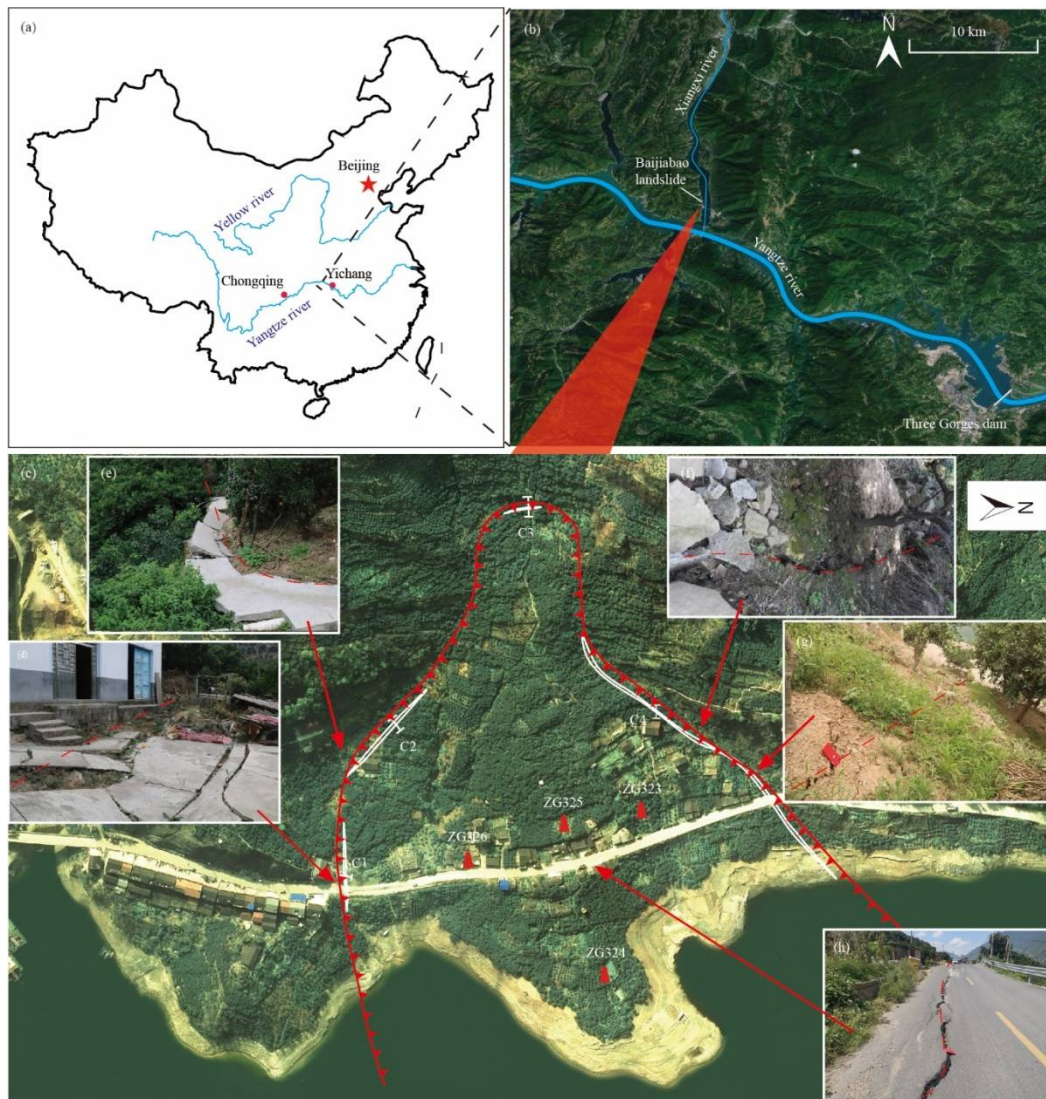
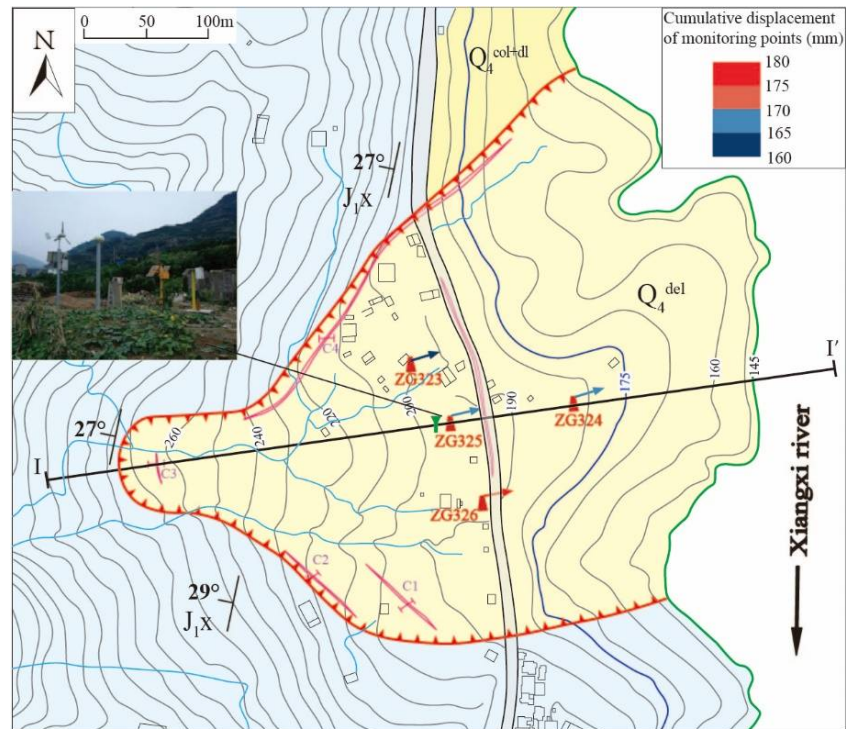


Figure 2. Location and oblique view of the Baijiabao landslide. (a) Study area location; (b) Landslide location; (c) Overall view of the Baijiabao landslide; (d) Crack along right boundary; (e) Crack on the footpath; (f) Crack on the farmland; (g) Crack along the left boundary; (h) Transverse crack on the road.



Legend
 Quaternary: Q_4^{del} Landslide deposits Q_4^{col+dl} Colluvium and Deluvium
 Lower Jurassic: J_1X Sandstone intercalated with mudstone of Xiangxi Formation
 27° Attitude J_1X Section I-I' --- Landslide boundary $ZG323$ Monitoring point
 $\text{---}C1$ Crack meter --- Rain gauge --- 175m RWL --- 145m RWL

Figure 3. The monitoring system and geological map of the Baijiabao landslide (colored arrows demonstrate the direction and magnitude of the monitoring points).

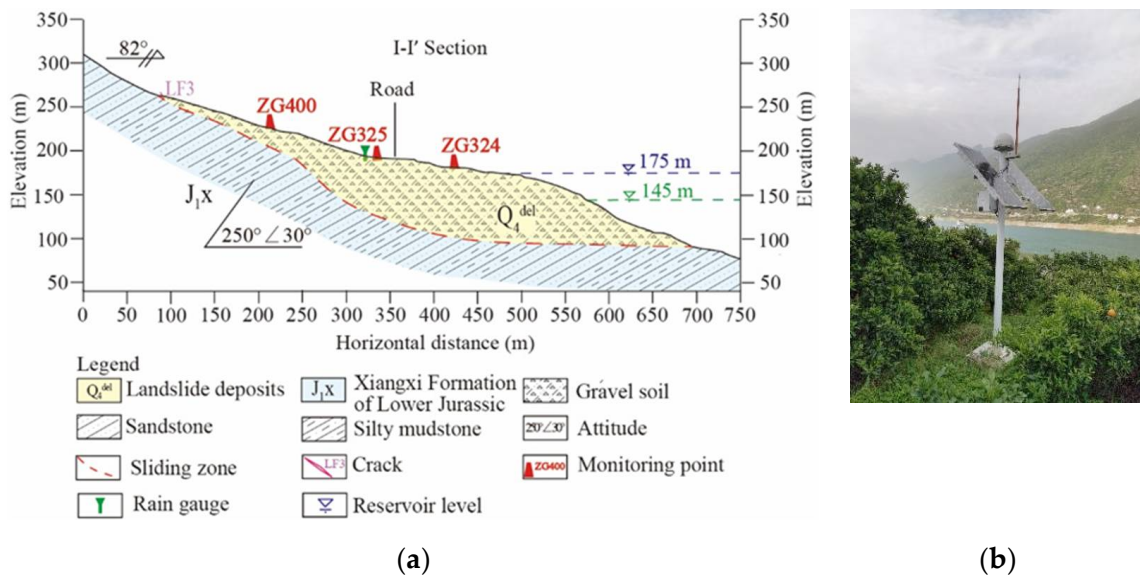


Figure 4. (a) Geological cross-section I-I'; (b) the GNSS monitoring station.

3.2. Deformation Characteristics

3.2.1. Deformation History

The reservoir was first impounded to 135 m, 156 m, and 175 m in 2003, 2006, and 2008, respectively. Then the RWL was cyclically operated between 145 and 175m every year. The site investigation is carried out every month and more frequently during the rainfall season since 2003, as part of the early warning system in the TGR area. Several discontinued cracks have shown up in the south flank and two cracks in the north flank on 22 June 2003 during the first impoundment of TGR. After a heavy rainfall event, the deformation intensified, and a series of large cracks emerged at the head of the landslide [32]. The road also subsided when the RWL first reached 135 m a.s.l. According to data from inclinometer ZK1 from October 2003 to July 2004, an obvious potential sliding band was detected 28 to 30 m underground, as shown in Figure 5. It indicates that the Baijiabao landslide has experienced an obvious movement above the sliding zone. Unfortunately, the casing of the inclinometer was cut off in August 2004 as a result of the continuous deformation of the landslide.

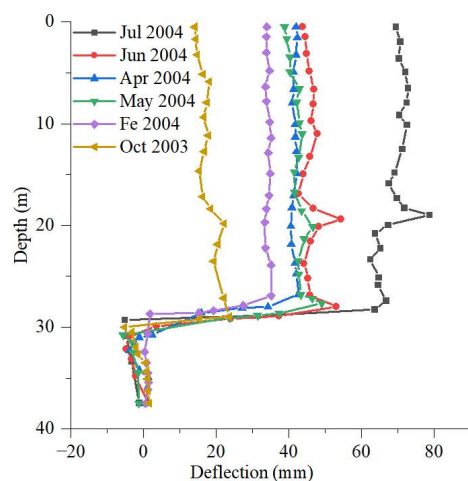


Figure 5. Movement of inclinometer ZK-1 at the upper part of the Baijiabao landslide.

During the rainfall season in 2008, a lengthways crack appeared on the road at the left boundary (Figure 2f). In July 2014, the right boundary crack C1 extended into the courtyard of the resident (Figure 6b). In 2015, the transverse crack showed up along the new road, and the road continuously sunk in the following years. The settlement is about 3 m by now (Figure 6c,d). In June 2020, an arc transverse crack, 20 m long and 1 to 10 cm wide, was observed on the new road which was rebuilt in July 2019 (Figure 6d). At the same time, the parts of the road on the left boundary started to sink again (Figure 6a). It is worth mentioning that the cracks on the left boundary open in July and close in October every year as shown in Figure 2g.

3.2.2. Characteristics of the Monitoring Data

The deformation trend of the Baijiabao landslide is established by the surficial monitoring instruments on the slope. Figure 7 displays the cumulative displacements of the Baijiabao landslide monitored by GNSS stations from 2006 to 2020. The displacement data illustrated that this landslide was in the stage of an overall movement toward the Xiangxi River, and the average movement direction is N74°E (Figure 3). The largest displacement monitoring point is ZG326 which occurs on the right part of the landslide. The smallest is ZG323 on the left part. The different parts of a landslide may present different velocities due to the micro-topographic features, especially for soil landslides [35]. Although the deformation magnitude is different, the trend is consistent. By far, the total displacement is up to 1.8 m and exhibits a dynamic step-like pattern. As shown in Figures 7 and 8, this landslide experiences fast movement toward the river typically in June or July every

year when the RWL decreases to the lowest level, exhibiting an intermittently moving pattern [36,37]. According to the field investigation, the cracks along the left boundary were opened in the process of the RWL water falling to 145 m. However, when the RWL is relatively high during the rest of the year, the slope moved slowly even backward slightly (the monthly displacements appeared negative) and the cracks in the left boundary were closed. The statistics of the annual displacement rates since 2006 in Figure 9 indicated that this landslide experienced an alternate movement from 2006 to 2015. In the past 5 years, the annual displacement has decreased, from 160 mm in 2015 to 40 mm in 2018. It seems like the landslide was gradually accommodated to the cycle of the reservoir.



Figure 6. Deformation characteristics in the field. (a) Crack along left boundary in 2021; (b) Crack along right boundary in 2021; (c) Transverse crack on the new road in 2021; (d) the sunken road in 2017.

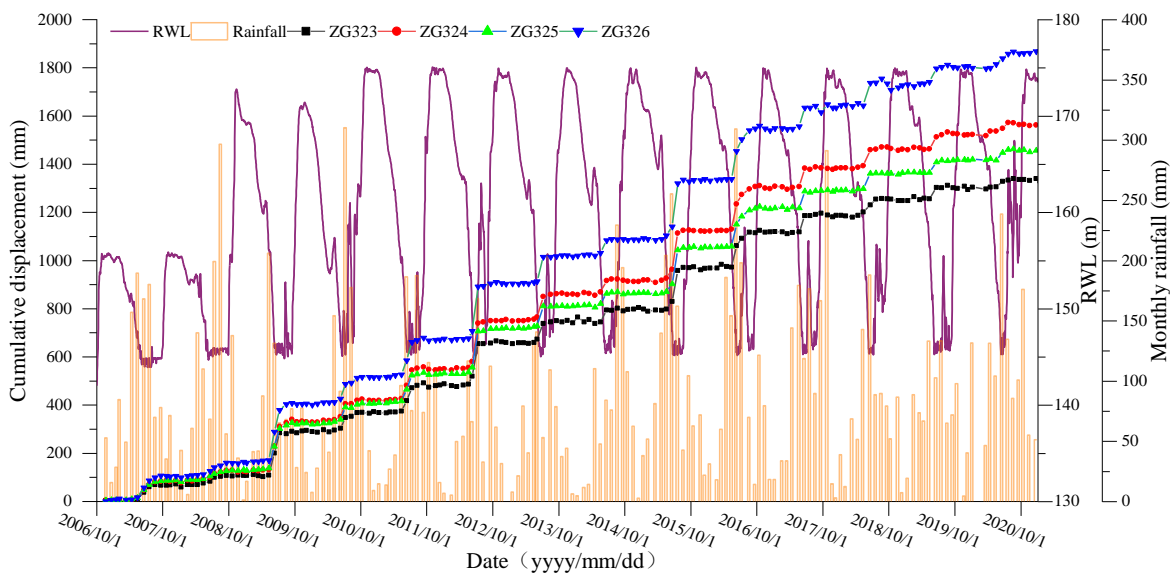


Figure 7. Time series of monitoring accumulative displacement, reservoir water level, and monthly rainfall.

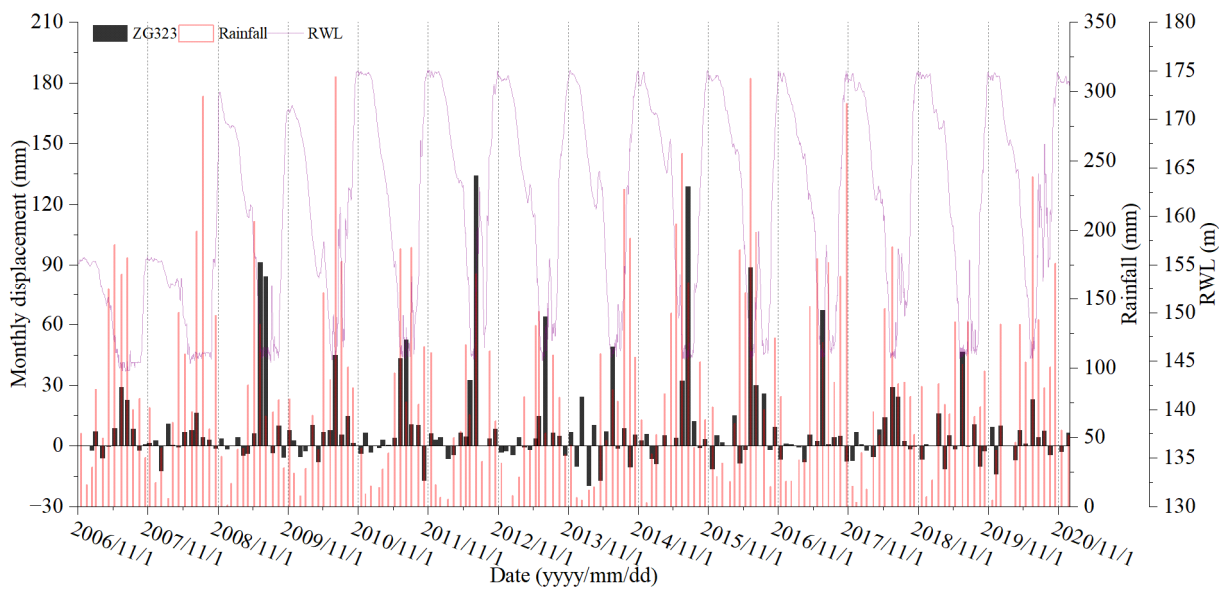


Figure 8. Monthly displacement corresponds to the reservoir water level and monthly rainfall.

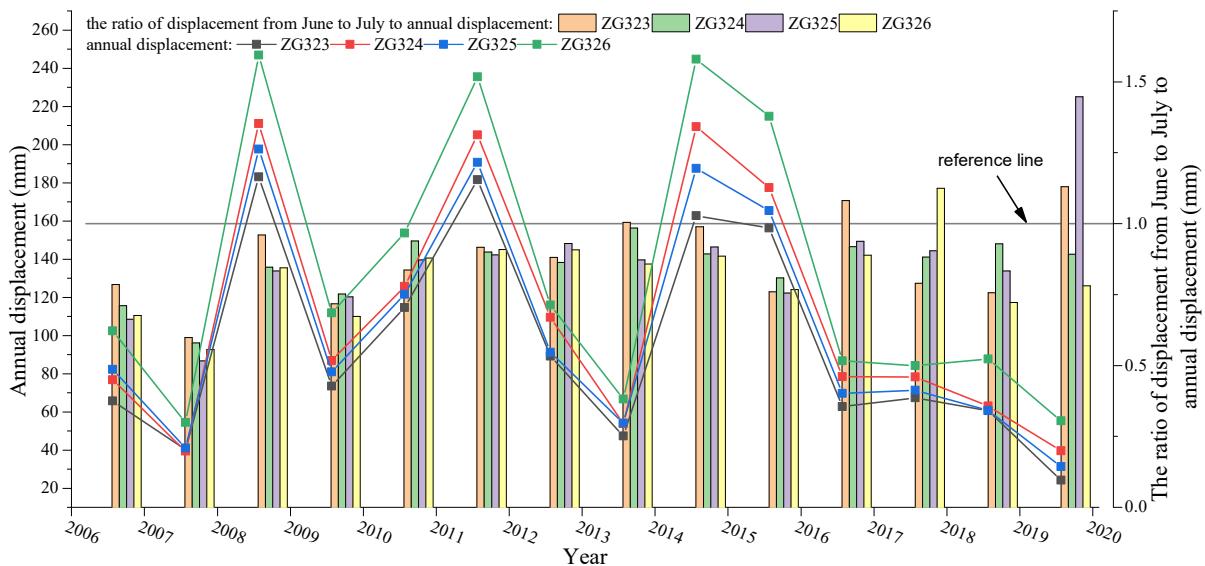


Figure 9. Annual displacement and the ratio of displacement from June to July to annual displacement.

The displacements of crack meter C1 to C4 were shown in Figure 10. Three accelerated events (confined by the cyan rectangle and labeled from A1 to A3) were revealed. In these events, the displacements increased sharply with a maximum displacement of approximately 100 mm with the RWL drawdown from 152 to 145 m in June. In contrast, the movement during the rest of the year was subtle unless stimulated by extreme events. Like the extreme rainfall event in October 2017, a long-duration rainfall from late September to October caused this deformation. This rainfall event activated many landslides in the Zigui county, TGR area (such as the Baibao landslide and the Tanjiwan landslide) [38]. The trend is highly consistent with the GNSS. But the magnitude is different: the displacement from April 2017 to January 2020 at C1, C2, and C4 were 273, 413, and 413 mm, respectively, whereas it is 187, 219, 197, and 252 mm for ZG323, ZG324, ZG325, and ZG326, respectively within the same period.

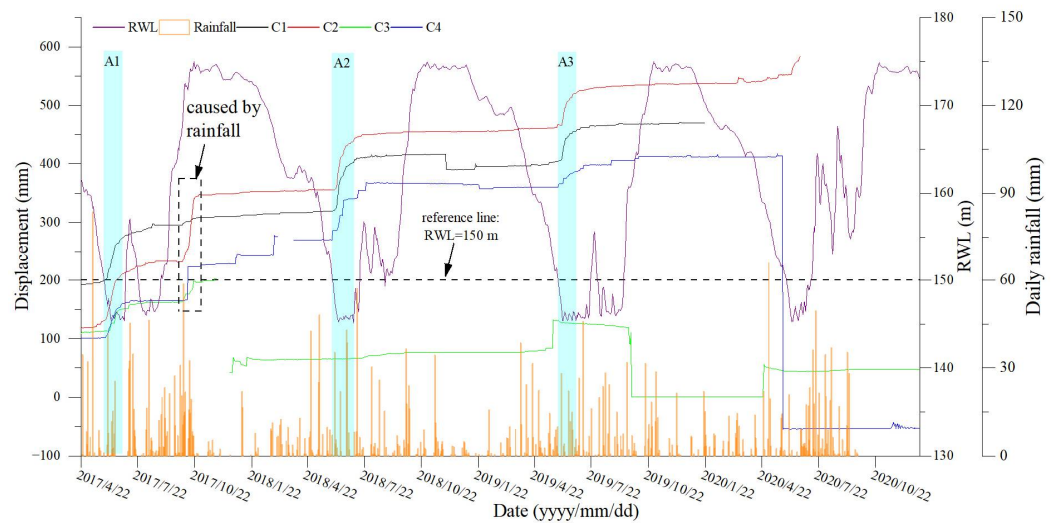


Figure 10. The displacement of crack meters C1, C2, C3, and C4.

3.3. Prediction of Landslide Displacement

The GPS monitoring point ZG324, which is located at the front of the profile I-I' of the Baijiabao landslide, was used for the establishment of the predicting model. According to the analyses before, the rainfall and the reservoir level impose an important effect on the landslide movement. Thus, the rainfall and RWL were also input into the proposed model.

Wavelet transform was adopted for de-noising to remove the monitoring error. The monitoring data from December 2006 to June 2016 were input into the model for training, the data from July 2016 to February 2019 were adopted for validation, and the remaining (from February 2019 to July 2020) were utilized to test the capability of the hybrid model.

3.3.1. Trend Displacement Prediction

The VMD decomposing method was applied to decompose the original total surface displacement into the trend part and the periodic part. The results are exhibited in Figure 11. It depicts that the trend displacement was an approximate monotonically increasing series. The trend displacement rate and the periodic displacement rate decreased in recent years. This phenomenon may be due to the strength–regain mechanisms in the reactive intermittently moving landslides [36,37]. Even though the strength of the sliding zone is reduced to the residual state during sliding, it could be recovered to some extent during a more stable period. Hence the displacement rate is decreasing. It has been recognized in other reactive landslides in the TGR area, such as the Muyubao landslide [33], and the Bazimen landslide [18].

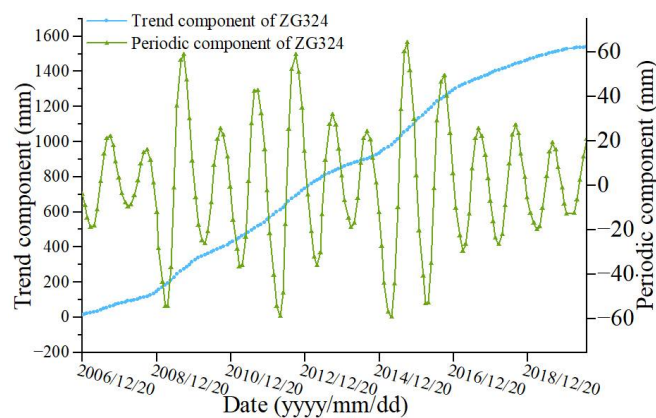


Figure 11. Decomposing results of the measured total displacement via VMD.

The trend displacement is dominated by the internal circumstances which represent the inherent behaviors of the landslides in the long term, such as geological conditions, structures, and materials [39]. It is popular to apply the double exponential smoothing method for the trend displacement predicting [40].

Figure 12a shows the result of the predicted trend displacement by the DES algorithm. Figure 12b illustrates the regression between the predicted and the measured value of the trend displacement, and the correlation coefficient is 1.00005 which indicates the excellent performance of this method.

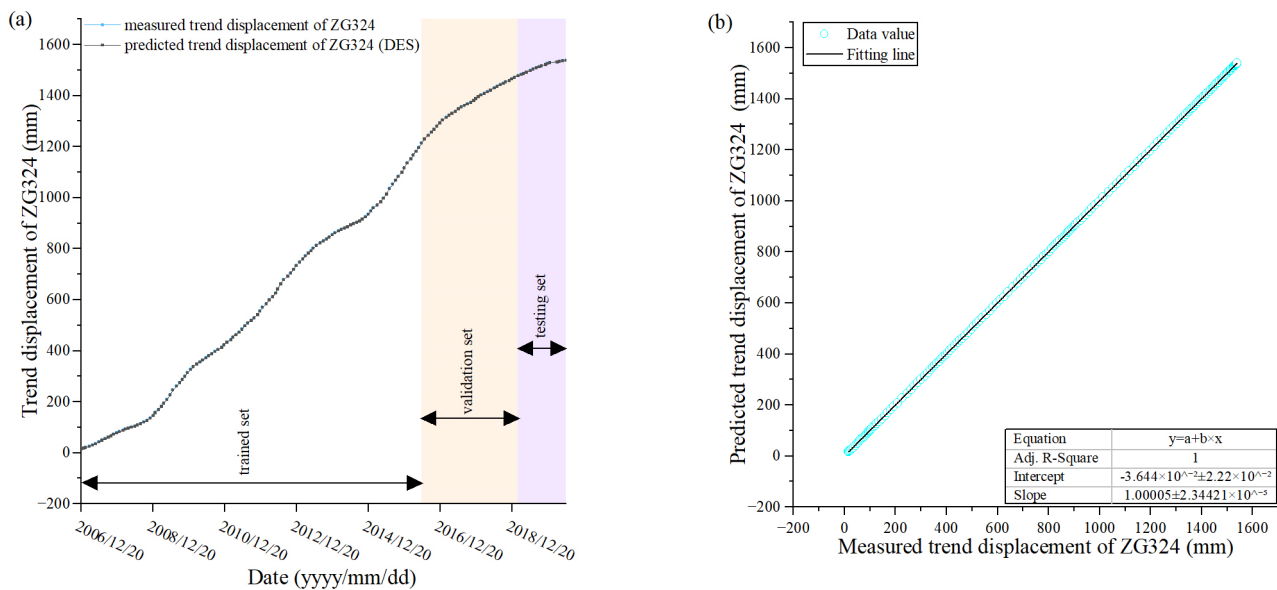


Figure 12. (a) Testing results of DES-model for trend displacement, (b) agreement of the predicted and measured trend displacement.

3.3.2. Periodic Displacement Prediction

It is important to predict the periodic displacement for obtaining the total displacement. Considering the analysis of the deformation characteristics above, the total displacement of the Baijiabao landslide was governed by the RWL and seasonal rainfall. Figure 13 demonstrates that the periodic displacement decreases or increases when the RWL is rising or falling. However, the pace does not match and there is a time lag between the periodic displacements and the RWL. Considering the dependence of the movement on the state evolution of the landslide and the external factors, six major influence factors were adopted, including the rainfall of the current month, the change of RWL during the last month, the RWL of the current month, the RWL of the last month, the RWL two months before, and the variation of the periodic displacement during last month.

Those major influences were input into the PSO–ELM model, and the predicting results are presented in Figure 14a. It illustrates that the shape of the periodic displacement was accurately captured and the crests and the valleys of the periodic displacements were predicted, which verifies that the reasonability and reliability of the input major influences in return. Figure 14b indicated that the correlation coefficient between the measured and predicted value is 0.99696 (close to 1 means high accuracy) and most of the predictors are concentrated in the 95% prediction band, which means PSO–ELM is a very effective method for periodic displacement prediction.

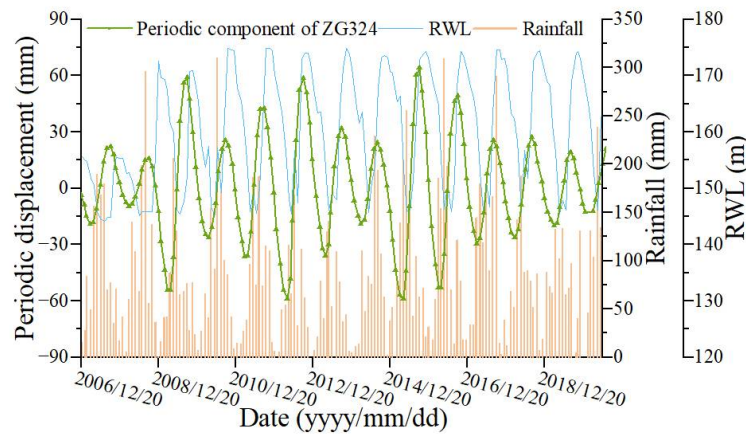


Figure 13. Relationships between the periodic displacement of ZG324, the rainfall, and the reservoir water level.

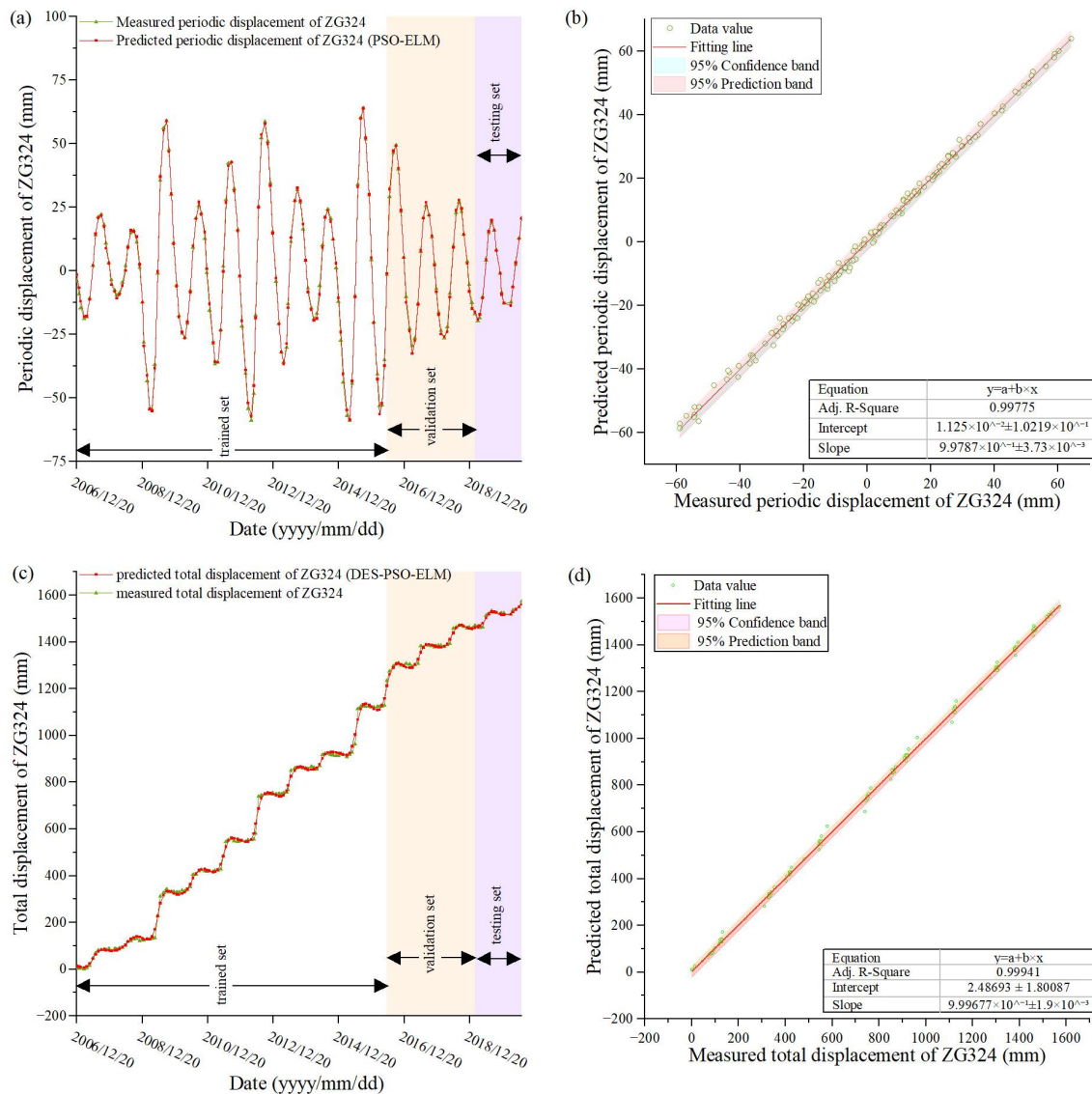


Figure 14. (a) Testing results of PSO-ELM for periodic displacement, (b) Agreement of the predicted and measured periodic displacement, (c) Total displacement predicted by DES-ELM and measured displacement, and (d) Agreement of the predicted and measured total displacement.

3.3.3. Total Displacement Prediction

The total displacement equals the summation of the predicted trend and periodic component. Figure 14c indicates that the proposed DES–PSO–ELM model has a splendid performance in the prediction of the measured displacement. Most predicted points were gathered in the 95% prediction band in Figure 14d i.e., the proposed hybrid machine learning model can be applied to predict the total displacement of landslides.

3.4. Comparison with Other Conventional Models

The periodic displacement was also predicted by the least square support vector machine and convolutional neural networks—gated recurrent units to assess the superiority of the proposed hybrid model. Figure 15 exhibits the prediction results of three comparison methods, it illustrates that the pattern of the periodic displacement was captured by three models, but the trough and crest vary a lot. The LSSVM and CNN–GRU model show less adaptability to the turn values.

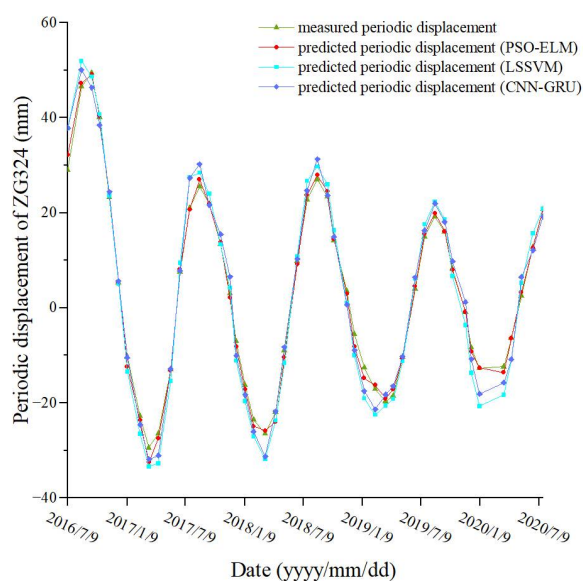


Figure 15. Predicted periodic displacement for different models.

Table 1 presents the performance results for three models. RMSE, MAE, and MAPE of the total data set for DES–PSO–ELM are the minimum for three models, 1.295%, 0.998, and 0.008 respectively. DES–PSO–ELM, in general, in training, validation, and testing is more excellent than the other two models.

Table 1. Comparison of different models for periodic displacement prediction (July 2016 to July 2020).

| Model | | RMSE | MAE | MAPE (%) | R ² |
|-------------|----------------|-------|-------|----------|----------------|
| DES–PSO–ELM | total | 1.295 | 0.998 | 0.008 | 1.000 |
| | training set | 1.340 | 1.041 | 0.012 | 1.000 |
| | validation set | 1.369 | 1.088 | 0.001 | 0.999 |
| | testing set | 0.657 | 0.512 | 0.001 | 0.991 |
| DES–LSSVM | total | 2.542 | 1.944 | 0.013 | 0.999 |
| | training set | 1.824 | 1.458 | 0.017 | 1.000 |
| | validation set | 3.829 | 3.207 | 0.002 | 0.989 |
| | testing set | 3.551 | 2.904 | 0.002 | 1.032 |
| DES–CNN–GRU | total | 2.409 | 1.811 | 0.015 | 1.000 |
| | training set | 2.045 | 1.535 | 0.021 | 1.000 |
| | validation set | 3.297 | 2.533 | 0.002 | 0.999 |
| | testing set | 2.708 | 2.350 | 0.002 | 0.961 |

4. Discussion

4.1. Effects of RWL

The movement of the Baijiabao landslide shows a remarkable response (the open and close of the crack) to the periodic operation of the reservoir, especially during the drawdown in Figure 6. Figure 7 illustrates that when the RWL was drawn down to about 150 m, the monthly displacement increased sharply and lasted for approximately 1 or 2 months every year. Figure 8 shows that the displacement from June to July accounted for more than 50 percent of the annual displacement every year and 75 percent most of the time. The proportion of ZG323, ZG325, and ZG326 exceeded 100 percent in some years which means the body of the landslide moved forward in these two months and backward in some other specific months when the RWL is higher.

The detailed examination of the monthly displacement rate scatters, in Figure 16, also suggested that fast movement scatters were mostly spread between 145 m and 152 m, and the majority of negative points are concentrated in the red rectangle when the RWL is higher than 160 m. In addition, the data show that the fast point only shows up when the RWL rate is between 0.2 and -0.6 m/day and mostly is characterized by the negative rate of RWL. It demonstrated that the low RWL during the drawdown (mainly from 152 to 150 m) has a favorable condition for the acceleration of the Baijiabao landslide while the high RWL (higher than 160 m) has a worse condition. 152 m during the drawdown could be an RWL threshold for deformation warning of this landslide.

4.2. Effects of Rainfall

Due to the low RWL phase being overlapped by the rain season, it is hard to analyze the relations between displacement and rainfall. Figure 17 shows that with the monthly rainfall rise, the monthly displacement did not show an obvious upward trend even at the same water level (the points in the same color). On the contrary, the RWL of the points with large displacement is low. It suggested that the monthly rainfall amount can not reflect the rainfall effect properly.

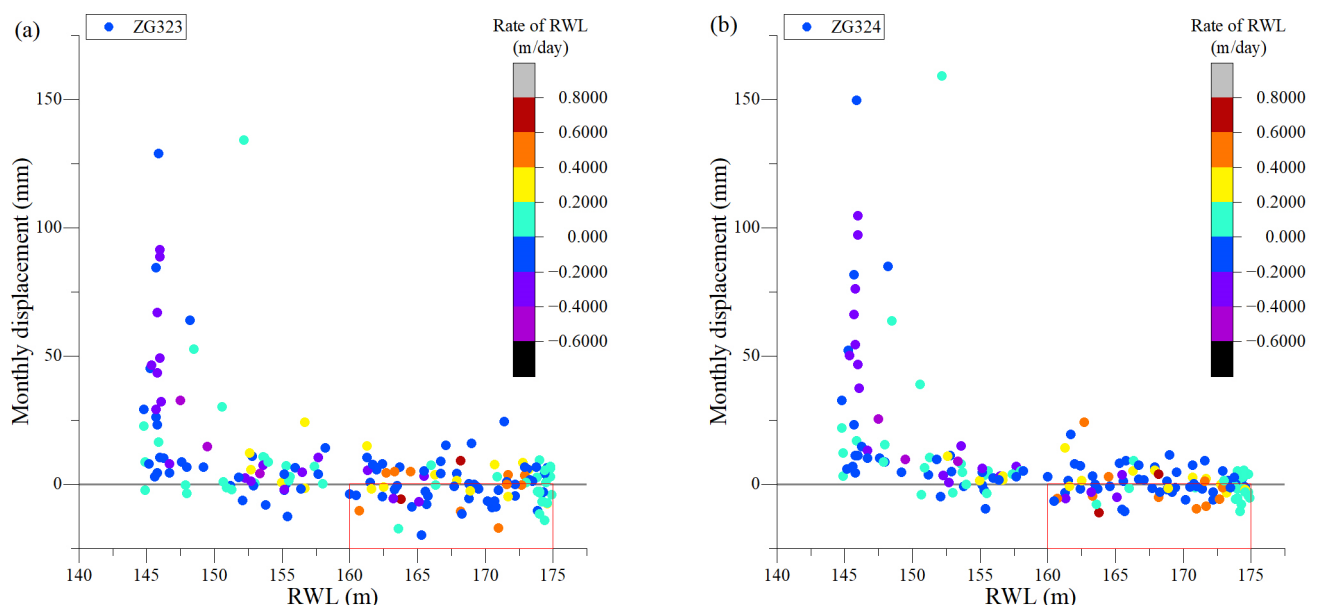


Figure 16. Cont.

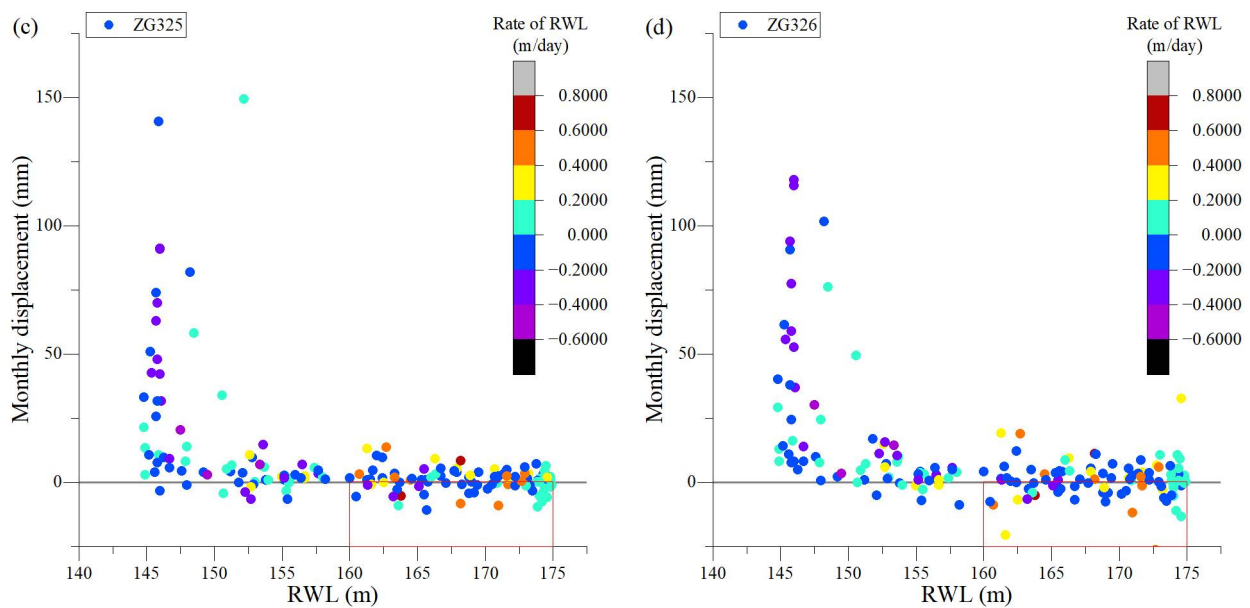


Figure 16. Effects of RWL on landslide displacement. (a) ZG323; (b) ZG324; (c) ZG325; (d) ZG326.

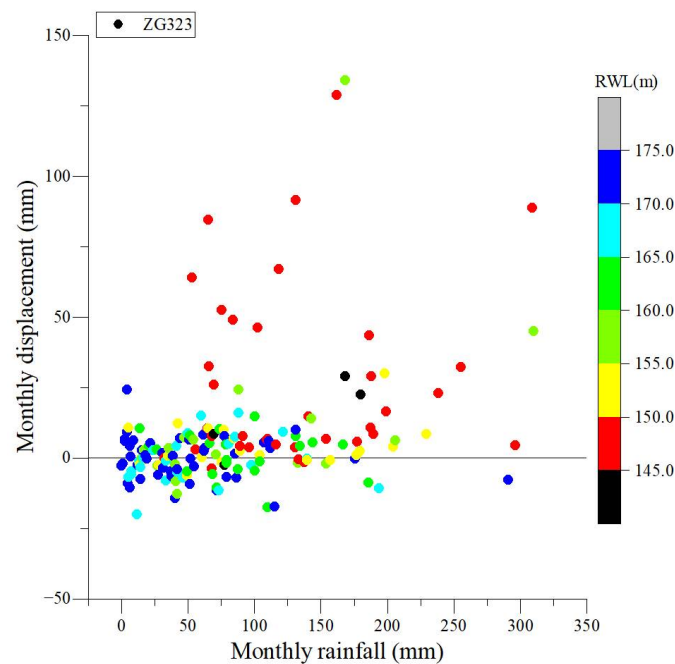


Figure 17. Effect of Rainfall on landslide displacement illustrated by ZG323.

As shown in Figure 10, the maximum daily rainfall of 83.4mm occurred on 11 May 2017 but the fast movement did not occur this month. The displacement increased fast after a 22-days long rainfall event in October 2017. The 22 days of cumulative rainfall from 27 September 2017 to 18 October 2017, is 280.4 mm which is the biggest 22 days of cumulative rainfall (DCR) from 2017 to 2020. This event caused many landslides in Zigui County [38]. The displacement of cracks started to increase on 2 October and the cumulative rainfall was about 120.3 mm. The increment was about 12 to 97 mm in this rainfall event. It suggested that long-duration-low-intensity rainfall has an impact on the stability of the Baijiabao landslide.

5. Conclusions

In this study, a hybrid machine learning model coupling double exponential smoothing, particle swarm optimization, and extreme learning machine were proposed. Applying this model, the displacement of the Baijiabao landslide in the TGR area was used for testing. The LSSVM and CNN-GRU models were used for comparison. The total landslide displacement can be predicted accurately with the proposed model which proved to be the best with RMSE of 1.295%, MAE of 0.998, MAPE of 0.008, and accuracy of 1.000.

The annual displacement of the Baijiabao landslide has decreased during the past five years, and the effect of the cycle of the reservoir on the stability has diminished. The primary external influences of the Baijiabao landslide are the fluctuation of the reservoir and the long-duration seasonal rainfall. The displacement from June to July accounts for more than 50% of the annual displacement. The rise of the reservoir has contributed to the stability of the Baijiabao landslide which was reflected by the displacement monitoring data. The RWL 152 m during the drawdown could be the deformation warning threshold of this landslide.

Author Contributions: All the authors participated in editing and reviewing the manuscript. X.Z., F.Z., M.D., Z.H. and J.L. conceived and designed the experiments; X.Z., F.Z., Z.H. and J.L. performed the experiments; F.Z. and M.D. carried out the field investigation; X.Z., F.Z., W.Z. and X.G. analyzed and interpreted the results. All authors have read and agreed to the published version of the manuscript.

Funding: This research was funded by the National Key R & D Program of China, grant number 2019YFC1509602, and the National Natural Science Foundation of China, grant number 42172303.

Data Availability Statement: Not applicable.

Acknowledgments: We thank the National Field Observation and Research Station of Landslides in the Three Gorges Reservoir Area of Yangtze River (<https://newtgls.ctgu.edu.cn> accessed on 8 June 2022) and Qinglin Yi in the Hubei Province Disaster Prevention and Mitigation Engineering Technology Research Center for making monitoring data available. All authors thank the reviewers for their constructive advice.

Conflicts of Interest: The authors declare no conflict of interest.

References

1. Wang, F.; Li, T. *Landslide Disaster Mitigation in Three Gorges Reservoir, China*; Springer: Berlin, Germany, 2009; p. 563.
2. Tang, H.; Wasowski, J.; Juang, C.H. Geohazards in the Three Gorges Reservoir Area, China—Lessons Learned from Decades of Research. *Eng. Geol.* **2019**, *261*, 105267. [[CrossRef](#)]
3. Tang, M.; Xu, Q.; Yang, H.; Li, S.; Iqbal, J.; Fu, X.; Huang, X.; Cheng, W. Activity Law and Hydraulics Mechanism of Landslides with Different Sliding Surface and Permeability in the Three Gorges Reservoir Area, China. *Eng. Geol.* **2019**, *260*, 105212. [[CrossRef](#)]
4. Yin, Y.; Wang, H.; Gao, Y.; Li, X. Real-Time Monitoring and Early Warning of Landslides at Relocated Wushan Town, the Three Gorges Reservoir, China. *Landslides* **2010**, *7*, 339–349. [[CrossRef](#)]
5. Jian, W.; Xu, Q.; Yang, H.; Wang, F. Mechanism and Failure Process of Qianjiangping Landslide in the Three Gorges Reservoir, China. *Environ. Earth Sci.* **2014**, *72*, 2999–3013. [[CrossRef](#)]
6. Shihabudheen, K.V.; Peethambaran, B. Landslide Displacement Prediction Technique Using Improved Neuro-Fuzzy System. *Arab. J. Geosci.* **2017**, *10*, 502. [[CrossRef](#)]
7. Wen, T.; Tang, H.; Wang, Y.; Lin, C.; Xiong, C. Landslide Displacement Prediction Using the GA-LSSVM Model and Time Series Analysis: A Case Study of Three Gorges Reservoir, China. *Nat. Hazards Earth Syst. Sci.* **2017**, *17*, 2181–2198. [[CrossRef](#)]
8. Lian, C.; Zeng, Z.; Yao, W.; Tang, H. Multiple Neural Networks Switched Prediction for Landslide Displacement. *Eng. Geol.* **2015**, *186*, 91–99. [[CrossRef](#)]
9. Hu, X.; Wu, S.; Zhang, G.; Zheng, W.; Liu, C.; He, C.; Liu, Z.; Guo, X.; Zhang, H. Landslide Displacement Prediction Using Kinematics-Based Random Forests Method: A Case Study in Jinping Reservoir Area, China. *Eng. Geol.* **2021**, *283*, 105975. [[CrossRef](#)]
10. Miao, F.; Wu, Y.; Xie, Y.; Li, Y. Prediction of Landslide Displacement with Step-like Behavior Based on Multialgorithm Optimization and a Support Vector Regression Model. *Landslides* **2018**, *15*, 475–488. [[CrossRef](#)]
11. Zhu, X.; Shu-Qi, M.A.; Qiang, X.U.; Liu, W.D. A WD-GA-LSSVM Model for Rainfall-Triggered Landslide Displacement Prediction. *J. Mt. Sci.* **2018**, *15*, 156–166. [[CrossRef](#)]

12. Han, H.; Shi, B.; Zhang, L. Prediction of Landslide Sharp Increase Displacement by SVM with Considering Hysteresis of Groundwater Change. *Eng. Geol.* **2021**, *280*, 105876. [[CrossRef](#)]
13. Li, H.; Xu, Q.; He, Y.; Deng, J. Prediction of Landslide Displacement with an Ensemble-Based Extreme Learning Machine and Copula Models. *Landslides* **2018**, *15*, 2047–2059. [[CrossRef](#)]
14. Liao, K.; Wu, Y.; Miao, F.; Li, L.; Xue, Y. Using a Kernel Extreme Learning Machine with Grey Wolf Optimization to Predict the Displacement of Step-like Landslide. *Bull. Eng. Geol. Environ.* **2020**, *79*, 673–685. [[CrossRef](#)]
15. Zhang, L.; Chen, X.; Zhang, Y.; Wu, F.; Chen, F.; Wang, W.; Guo, F. Application of GWO-ELM Model to Prediction of Caojiatuo Landslide Displacement in the Three Gorge Reservoir Area. *Water* **2020**, *12*, 1860. [[CrossRef](#)]
16. Jiang, Y.; Xu, Q.; Lu, Z.; Luo, H.; Liao, L.; Dong, X. Modelling and Predicting Landslide Displacements and Uncertainties by Multiple Machine-Learning Algorithms: Application to Baishuihe Landslide in Three Gorges Reservoir, China. *Geom. Nat. Hazards Risk* **2021**, *12*, 741–762. [[CrossRef](#)]
17. Xu, S.; Niu, R. Displacement Prediction of Baijiabao Landslide Based on Empirical Mode Decomposition and Long Short-Term Memory Neural Network in Three Gorges Area, China. *Comput Geosci.* **2018**, *111*, 87–96. [[CrossRef](#)]
18. Yang, B.; Yin, K.; Lacasse, S.; Liu, Z. Time Series Analysis and Long Short-Term Memory Neural Network to Predict Landslide Displacement. *Landslides* **2019**, *16*, 677–694. [[CrossRef](#)]
19. Jiang, H.; Li, Y.; Zhou, C.; Hong, H.; Glade, T.; Yin, K. Landslide Displacement Prediction Combining LSTM and SVR Algorithms: A Case Study of Shengjibao Landslide from the Three Gorges Reservoir Area. *Appl. Sci.* **2020**, *10*, 7830. [[CrossRef](#)]
20. Li, L.; Zhou, H.; Liu, H.; Zhang, C.; Liu, J. A Hybrid Method Coupling Empirical Mode Decomposition and a Long Short-Term Memory Network to Predict Missing Measured Signal Data of SHM Systems. *Struct. Health Monit.* **2021**, *20*, 1778–1793. [[CrossRef](#)]
21. Du, J.; Yin, K.; Lacasse, S. Displacement Prediction in Colluvial Landslides, Three Gorges Reservoir, China. *Landslides* **2013**, *10*, 203–218. [[CrossRef](#)]
22. Huang, F.; Huang, J.; Jiang, S.; Zhou, C. Landslide Displacement Prediction Based on Multivariate Chaotic Model and Extreme Learning Machine. *Eng. Geol.* **2017**, *218*, 173–186. [[CrossRef](#)]
23. Zhang, Y.; Wang, X.; Tang, H. An improved Elman neural network with piecewise weighted gradient for time series prediction. *Neurocomputing* **2019**, *359*, 199–208. [[CrossRef](#)]
24. Zhang, J.; Tang, H.; Wen, T.; Ma, J.; Tan, Q.; Xia, D.; Liu, X.; Zhang, Y. A Hybrid Landslide Displacement Prediction Method Based on CEEMD and DTW-ACO-SVR-Cases Studied in the Three Gorges Reservoir Area. *Sensors* **2020**, *20*, 4287. [[CrossRef](#)] [[PubMed](#)]
25. Xie, Y.; Lou, Y. Hydrological Time Series Prediction by ARIMA-SVR Combined Model Based on Wavelet Transform. In Proceedings of the 2019 3rd International Conference on Innovation in Artificial Intelligence, Suzhou, China, 15–18 March 2019; Association for Computing Machinery: New York, NY, USA, 2019; pp. 243–247.
26. Dragomiretskiy, K.; Zosso, D. Variational Mode Decomposition. *IEEE Trans. Sign. Process.* **2014**, *62*, 531–544. [[CrossRef](#)]
27. Kaloop, M.R.; Kim, D. De-Noiseing of GPS Structural Monitoring Observation Error Using Wavelet Analysis. *Geom. Nat. Hazards Risk* **2016**, *7*, 804–825. [[CrossRef](#)]
28. Li, Y.; Xu, C.; Yi, L.; Fang, R. A Data-Driven Approach for Denoising GNSS Position Time Series. *J. Geod.* **2018**, *92*, 905–922. [[CrossRef](#)]
29. Tsividis, Y. Event-Driven Data Acquisition and Digital Signal Processing—A Tutorial. *IEEE Trans. Circuits Syst. II Express Briefs.* **2010**, *57*, 577–581. [[CrossRef](#)]
30. Kennedy, J.; Eberhart, R. Particle Swarm Optimization. In Proceedings of the ICNN'95—International Conference on Neural Networks, Perth, WA, Australia, 27 November–1 December 1995; Volume 4, pp. 1942–1948.
31. Huang, G.-B.; Zhu, Q.-Y.; Siew, C.-K. Extreme Learning Machine: Theory and Applications. *Neurocomputing* **2006**, *70*, 489–501. [[CrossRef](#)]
32. Huang, B.; Chen, X. Deformation failure mechanism of Baijiabao landslide in Xiangxi River Valley. *Chin. J. Geotech. Eng.* **2007**, *29*, 938–942. (In Chinese) [[CrossRef](#)]
33. Deng, M.; Zhou, J.; Yi, Q.; Zhang, F.; Han, B.; Li, Z. Characteristics and mechanism of deformation of chair-shaped soil landslides in Three Gorges Reservoir area. *Chin. J. Geot. Eng.* **2020**, *42*, 1296–1303. (In Chinese) [[CrossRef](#)]
34. Huadi Company. *Geological Report on Baijiabao Landslide for Early Warning and Monitoring in Zigui, TGR*; Technical Report; Huadi Company: Chengdu, China, 2007. (In Chinese)
35. Xu, Q.; Peng, D.; Fan, X.; Zhu, X.; He, C. Presenting Some Successful Cases of Regional Landslides Early Warning Systems in China. In *Understanding and Reducing Landslide Disaster Risk: Volume 3 Monitoring and Early Warning*; Casagli, N., Tofani, V., Sassa, K., Bobrowsky, P.T., Takara, K., Eds.; ICL Contribution to Landslide Disaster Risk Reduction; Springer International Publishing: Cham, Switzerland, 2021; pp. 279–286. ISBN 978-3-030-60311-3.
36. Angeli, M.; Gasparetto, P.; Bromhead, E. *Strength-Regain Mechanisms in Intermittently Moving Slides*; Balkema: Leiden/Amsterdam, The Netherlands, 2004; pp. 689–696. ISBN 04-1535-667-9.
37. Gibo, S.; Egashira, K.; Ohtsubo, M.; Nakamura, S. Strength Recovery from Residual State in Reactivated Landslides. *Géotechnique* **2002**, *52*, 683–686. [[CrossRef](#)]
38. Zhang, F.; Deng, M.; Yi, Q.; Lu, S.; Zheng, W.; Huang, H.; Zhu, X. Deformation Characteristics and Thresholds of the Tanjiawan Landslide in the Three Gorges Reservoir Area. *China J. Mt. Sci.* **2022**, *19*, 1370–1385. [[CrossRef](#)]

39. Zhu, X.; Xu, Q.; Tang, M.; Nie, W.; Ma, S.; Xu, Z. Comparison of Two Optimized Machine Learning Models for Predicting Displacement of Rainfall-Induced Landslide: A Case Study in Sichuan Province, China. *Eng. Geol.* **2017**, *218*, 213–222. [[CrossRef](#)]
40. Xing, Y.; Yue, J.; Chen, C.; Cai, D.; Hu, J.; Xiang, Y. Prediction Interval Estimation of Landslide Displacement Using Adaptive Chicken Swarm Optimization-Tuned Support Vector Machines. *Appl. Intell.* **2021**, *51*, 8466–8483. [[CrossRef](#)]